DMD Fast Forward. Published on March 1, 2012 as DOI: 10.1124/dmd.111.043596
DMD Fast Forward. Published on March 1, 2012 as doi:10.1124/dmd.111.043596
This article has not been copyedited and formatted. The final version may differ from this version.

DMD #43596

In Vitro and In vivo Metabolism and Pharmacokinetics of BMS-562086, a Potent and Orally Bioavailable Corticotropin Releasing Factor-1 (CRF_1) Receptor Antagonist

Lian Zhou, Randy C. Dockens, Peggy Liu-Kreyche, Scott J. Grossman and Ramaswamy A. Iyer

Department of Pharmaceutical Candidate Optimization (L.Z, P.L.-K., S.J.G, R.A.I.), Discovery Medicine and Clinical Pharmacology (R.C.D.), Bristol-Myers Squibb Co., Princeton, New Jersey, 08540, USA

Downloaded from dmd.aspetjournals.org at ASPET Journals on April 19, 2024

Copyright 2012 by the American Society for Pharmacology and Experimental Therapeutics.

DMD Fast Forward. Published on March 1, 2012 as DOI: 10.1124/dmd.111.043596
This article has not been copyedited and formatted. The final version may differ from this version.

Running Title: **Metabolism and Pharmacokinetics of BMS-562086**

Corresponding Author: Lian Zhou

Bristol-Myers Squibb Co.

P.O. Box 4000

Princeton, NJ 08543

Tel: (609) 252-4037

Fax: (609) 252-6802

Lian.zhou@bms.com

Number of Text Pages: 45

Number of Tables: 2

Number of Figures: 7

Number of References: 15

Number of Words in the Abstract: 209

Number of Words in the Introduction: 642

Number of Words in the Discussion: 1320

ABBREVIATIONS: CRF, corticotropin releasing factor; ADME, absorption, distribution, metabolism and excretion; BDC, bile-duct cannulated; HPLC, high-performance liquid chromatography; LC/MS/MS, liquid chromatography with tandem mass spectrometry; C_{max}, maximum observed concentration; T_{max}, time of maximum observed concentration; AUC(INF), area under the plasma concentration-time curve from time zero extrapolated to infinite time; $T_{1/2}$, terminal elimination half life; CL, clearance; V_z, terminal volume of distribution; F, oral bioavailability.

Downloaded from dmd.aspetjournals.org at ASPET Journals on April 19, 2024

DMD Fast Forward. Published on March 1, 2012 as DOI: 10.1124/dmd.111.043596
This article has not been copyedited and formatted. The final version may differ from this version.

ABSTRACT

The absorption, distribution, metabolism and excretion (ADME), and the pharmacokinetic characteristics of BMS-562086 (pexacerfont; DPC-A69448) were investigated in vitro and in animals to support its clinical development. BMS-562086 was orally bioavailable in rats, dogs and chimpazees, with an absolute oral bioavailability of 40.1%, 58.8% and 58.5%, respectively. BMS-562086 was extensively metabolized in hepatocytes from all species and completely metabolized in rats. The primary biotransformation pathways found for BMS-562086 in both liver microsomal and hepatocyte preparations and in rats were similar. These included *O*-demethylation, hydroxylation at the *N*-alkyl side chain and *N*-dealkylation. Multiple CYP P450s including CYP3A4/5 were involved in the metabolic clearance of BMS-562086. Both renal and biliary excretion played a significant role in elimination of the metabolites of BMS-562086. The involvement of other metabolic enzymes in addition to CYP3A4/5 in elimination of BMS-562086 suggests a reduced potential for drug-drug interaction through modulation of CYP3A4/5. Chimpanzees proved to be a good animal model in predicting BMS-562086 human clearance. Virtual clinical trials performed with the SimCYP population-based ADME simulator suggested that a minimum dose of 100 mg daily would provide sufficient drug exposure to achieve plasma concentrations above the projected human efficacious plasma concentration of BMS-562086 (>500 nM). In summary, BMS-562086 exhibited favorable ADME and pharmacokinetic properties for further development.

Downloaded from dmd.aspetjournals.org at ASPET Journals on April 19, 2024

DMD Fast Forward. Published on March 1, 2012 as DOI: 10.1124/dmd.111.043596
This article has not been copyedited and formatted. The final version may differ from this version.

INTRODUCTION

Corticotropin releasing factor subtype 1 (CRF_1) receptor mediates stress-induced activation of the hypothalamic-pituitary-adrenal axis (Owens and Nemeroff, 1991; Smagin and Dunn, 2000). In nonclinical studies, CRF_1, a pituitary adrenocorticotrophic hormone secretagogue and a neurotransmitter, played a pivotal role in the regulation of endocrine, autonomic and behavioral responses to stress (Owens and Nemeroff, 1991; Smagin and Dunn, 2000). Intracerebro ventricular administration of CRF_1 to rats generated many of the behavioral and physiological effects induced by stress. Mice which are null for the CRF_1 gene exhibited a reduced endocrine response to psychological stressors (Owens and Nemeroff, 1991; Smagin and Dunn, 2000). In addition, nonclinical studies suggested that CRF_1 antagonists are active in the treatment of irritable bowel syndrome (IBS), a stress related disorder (Sweetser, et al., 2011). Some clinical studies have implicated CRF in the pathophysiology of both depression and anxiety. An elevated level of CRF_1 in cerebrospinal fluid is observed in patients with anorexia nervosa, obsessive compulsive disorder and posttraumatic stress disorder (Coric, et al., 2010). In patients with IBS, subjects who displayed increased sensitivity to exogenous CRF_1 were more likely to suffer abdominal pain and hypermotility compared to healthy cohorts (Fukudo et al., 1998).

BMS-562086 {exacerfont; DPC-A69448; 8-(6-methoxy-2-methyl-3-pyridinyl)-2,7-dimethyl-*N*-[(1*R*)-1-methylpropyl]pyrazolo(1,5-a)-1,3,5-triazin-4-amine} is a selective

Downloaded from dmd.aspetjournals.org at ASPET Journals on April 19, 2024

DMD Fast Forward. Published on March 1, 2012 as DOI: 10.1124/dmd.111.043596
This article has not been copyedited and formatted. The final version may differ from this version.

CRF_1 receptor antagonist. It demonstrates a potent and specific inhibitory effect (IC_{50} = 6.1 ± 0.6 nM) toward human CRF_1 receptor and has greater than 1000-fold lower affinity (IC_{50} > 1000 nM) for the CRF-binding protein and biogenic amine receptors (Gilligan, et al., 2009). It is active in rats (1 to 10 mg/kg, orally) in the defensive withdrawal and elevated plus maze models of anxiety (Gilligan, et al., 2009).

An examination of the absorption, distribution, metabolism and excretion (ADME), and the pharmacokinetic characteristics of a drug candidate are essential for its successful development. Pre-clinical ADME studies can provide early information on a variety of properties, including permeability, plasma protein binding, metabolic soft spots, potential formation of reactive metabolites, metabolic pathways in different species, possible metabolites formed in humans, and potential for drug-drug interactions. Furthermore, knowing the biotransformation reactions that a drug molecule may be subjected to helps in the design and conduct of safety studies for new chemical entities (Humphreys and Unger, 2006).

The ADME properties of a drug molecule influence its pharmacokinetics in animal species and humans. The pharmacokinetic data can be extrapolated from animals to predict quantitatively the likely behavior in humans, since many of the basic processes controlling pharmacokinetics are similar across species. Frequently, a reasonable dose-correlated plasma pharmacokinetic profile can further be simulated in humans. Hence, an understanding of the ADME and pharmacokinetic properties of a compound is critical in improving the chances of selecting not only the most promising drug candidate but also the most appropriate targeted doses to be tested in humans.

Downloaded from dmd.aspetjournals.org at ASPET Journals on April 19, 2024

DMD Fast Forward. Published on March 1, 2012 as DOI: 10.1124/dmd.111.043596
This article has not been copyedited and formatted. The final version may differ from this version.

In this study, the ADME and pharmacokinetic properties of BMS-562086 were investigated in vitro and in animals to support its clinical development as an orally effective agent intended for the treatment of depression, anxiety disorders, and IBS. The metabolism of BMS-562086 was compared in mouse, rat, dog, monkey and human liver microsomes and hepatocytes. The metabolic profiles and routes of excretion of BMS-562086-related components were identified in bile-duct cannulated (BDC) rats. The permeability of BMS-562086 was examined in Caco-2 cells and its pharmacokinetic properties determined in rats, dogs and chimpanzees. Rats and dogs were studied because they are the two species used for long-term toxicology evaluations. Chimpanzees are viewed as a good pharmacokinetic model since their size and many of the physiological relationships that affect drug clearance, such as organ blood flow, are similar to those in humans (Wong, et al., 2004). Furthermore, SimCYP population-based ADME simulator was used to make extrapolation to human pharmacokinetics by incorporating both the in vitro ADME and animal pharmacokinetic data, and the population-specific variability. Virtual clinical trials were performed to simulate the plasma pharmacokinetic profiles in humans.

Downloaded from dmd.aspetjournals.org at ASPET Journals on April 19, 2024

DMD Fast Forward. Published on March 1, 2012 as DOI: 10.1124/dmd.111.043596
This article has not been copyedited and formatted. The final version may differ from this version.

MATERIALS AND METHODS

Chemicals and Biologicals. BMS-562086, [^{14}C]BMS-562086 (30 μCi/mg, radiochemical purity >99%, chemical purity >99%), $^{13}CD_3$-BMS-562086, and the reference standards for its three metabolites, DPH-123554 (*O*-demethylated metabolite), DPH-124921 (*N*-dealkylated metabolite) and BMS-572273 (*N*-dealkylated and hydrolyzed metabolite) were synthesized by Bristol-Myers Squibb Research and Development (Princeton, NJ). Caco-2 cells were obtained from the American Type Culture Collection (Rockville, MD). Dulbecco's Modified Eagle's Medium, N-2-hydroxyethylpiperazine-N'-2-ethanesulfonic acid (HEPES), nonessential amino acids, L-glutamine, penicillin-G, and streptomycin were purchased from GIBCO/Invitrogen (Grand Island, NY). Heat-inactivated fetal bovine serum was obtained from GIBCO/Invitrogen. Rat tail collagen-type I was purchased from BD Biosciences (Franklin lakes, NJ). 24-Well Transwell® plates (surface area of 0.33 cm^2) with a polycarbonate membrane (3.0 μm pore size) were purchased from Corning (Corning, NY). Hank's balanced salt solution was purchased from Sigma Chemical Co. (St. Louis, MO). Acetic acid was purchased from Mallinckrodt Baker (Phillipsburg, NJ). Calcium chloride, 7-ethoxycoumarin, glucose, 7-hydroxycoumarin, Krebs-Henseleit buffer modified salt, sodium bicarbonate, sodium hydroxide, trepan blue solution (0.4%), NADPH and β-glucuronidase (Type HA-4, from Helix aspersa) were purchased from

Downloaded from dmd.aspetjournals.org at ASPET Journals on April 19, 2024

DMD Fast Forward. Published on March 1, 2012 as DOI: 10.1124/dmd.111.043596
This article has not been copyedited and formatted. The final version may differ from this version.

Sigma-Aldrich (St. Louis, MO). Ecolite™ liquid scintillation cocktail was purchased from MP Biomedicals (Solon, OH). Deionized water was prepared with a MilliQplus ultrapure water system (Millopore Corporation, Bedford, MA). All other chemicals used were reagent grade or better. Frozen rat, dog and human sera were obtained from Bioreclamation, Inc. (Hicksville, NY). Pooled liver microsomes were purchased from Gentest Co. Woburn, MA. Hepatocytes from male beagle dogs (fresh), male cynomolgus monkeys (cryopreserved) and humans (cryopreserved from three donors) were obtained from In Vitro Technologies (Baltimore, MA). Freshly isolated mouse and rat hepatocytes were provided by Technical Support Unit, Bristol-Myers Squibb Research and Development

Permeability across Caco-2 Cell Monolayers. Caco-2 cells at passage 50-60 were seeded on polycarbonate membranes of 24-Well Transwell® at a density of 60,000 cells/cm^2. The cells were cultured for 21-25 days in culture medium consisting of Dulbecco's Modified Eagle's Medium supplemented with 10% fetal bovine serum, 0.5 mM HEPES, 1% nonessential amino acids, 1% L-glutamine, 100 U/mL penicillin-G, and 100 μg/mL streptomycin. Prior to the permeability studies, apical (AP) and basolateral (BL) medium were replaced with transport buffer (Hanks Balanced Salt Solution supplemented with 2% N,N-dimethylacetamide, pH 7.4). AP to BL permeability study was initiated by replacing the AP medium with the transport buffer containing 25 μM BMS-562086. All permeability experiments were performed at 37^0C.

Downloaded from dmd.aspetjournals.org at ASPET Journals on April 19, 2024

DMD Fast Forward. Published on March 1, 2012 as DOI: 10.1124/dmd.111.043596
This article has not been copyedited and formatted. The final version may differ from this version.

Transepithelial electrical resistance (TEER) values were measured to assess cell monolayer integrity. TEER values were obtained both at the beginning and end of each experiment. Only wells with TEER values between 400-500 Ω cm^2 throughout the experiment were used in the studies. Mannitol (25 μM or 100 μM) transport experiments were performed in the same manner as other transport experiments. Mannitol served as a probe of the Caco-2 cell monolayer integrity (Zhou, et al., 2002).

Protein Binding in Serum. In vitro protein binding of BMS-562086 in rat, dog and human serum was determined by equilibrium dialysis. BMS-562086 in acetonitrile stock solution was added into serum to final concentrations of 12.8, 25.6 and 38.5 μM. The three concentrations represent the projected parent concentrations to be studied in pre-clinical and clinical investigations. Serum samples were dialyzed against 134 mM phosphate buffer (pH 7.4) in a dialysis membrane (Amika Corp., Holliston, MA) with a 10,000 Da molecular weight cutoff. The dialysis cells (Spectrum, Laguna Hills, CA) were rotated at 20 rpm in a water bath maintained at 37°C for 3 h. At the end of incubation, aliquots (100 μl) of buffer were taken and mixed with equal volume of serum of the species under investigation. Aliquots (20 μl) of serum samples were taken and mixed with a matrix (180 μl) contained blank serum of the species under investigation: phosphate buffer (0.134 M, pH 7.4) (1:1 v/v). The final percentage of unbound drug was expressed as the concentration in buffer divided by the concentration in serum. Serum stability of BMS-562086 was also measured with these serum samples over the 3-h incubation period.

Downloaded from dmd.aspetjournals.org at ASPET Journals on April 19, 2024

DMD Fast Forward. Published on March 1, 2012 as DOI: 10.1124/dmd.111.043596
This article has not been copyedited and formatted. The final version may differ from this version.

Hepatocyte Incubations. The cell viabilities were checked with the Trypan Blue exclusion method and a hemocytometer. The viability prior to the incubation for mouse, rat, dog, monkey and human hepatocytes were 71%, 88%, 91%, 68% and 78%, respectively. The cells were diluted with freshly prepared Krebs-Henseleit buffer to give a final concentration of 1.0×10^6 cells/ml. The hepatocyte incubations with BMS-562086 (25 μM) were performed in 4 ml volumes in open 20 ml glass scintillation vials in duplicate. The incubations were conducted on an orbital shaker (80 rpm) in a humidified NAPCO CO_2 6000 incubator (VWR, West Chester, PA) maintained under an oxygen/carbon dioxide (95/5) atmosphere at 37°C for 3 h. The positive control incubations with 7-ethoxycoumarin (7-EC) and 7-hydroxycoumarin (7-HC) were performed at 100 μM. A negative control, in the absence of the hepatocytes, was also performed. A vial of hepatocyte suspension, with no compound added, was included to check for viability at 1 h and 3 h. The incubations were stopped after 3 h by adding 1 volume of ice-cold acetonitrile. The reaction mixtures were sonicated for 5 min in a Branson 5210 sonicator and then centrifuged at 5000 rpm for 10 min. The supernatant fractions were analyzed by LC/MS/MS.

Microsomal Incubations. For the purpose of metabolite identification, a higher BMS-562086 concentration (100 μM) was used in the mouse, rat, dog, monkey and human liver microsomal incubations. The concentrations of microsomal proteins, NADPH and phosphate buffer were 1 mg/ml, 1 mM and 100 mM, respectively. Incubations were initiated by addition of NADPH to the assay mixture. The incubations were carried out in 5 ml glass test tubes at 37°C for 1 h in a shaking water bath. They were performed in

Downloaded from dmd.aspetjournals.org at ASPET Journals on April 19, 2024

DMD Fast Forward. Published on March 1, 2012 as DOI: 10.1124/dmd.111.043596
This article has not been copyedited and formatted. The final version may differ from this version.

duplicate at a final volume of 2 ml. Three control incubations were done: incubation in the absence of the microsomal protein, incubation in the absence of the cofactor NADPH, and incubation with 7-ethoxycoumarin (100 μM) as a positive control. Incubations were stopped by cooling on ice followed by addition of 2 ml acetonitrile. The incubation mixtures were then centrifuged at 5000 rpm for 10 min. The supernatants were removed and evaporated to near dryness under a stream of nitrogen. The residues were reconstituted in 0.5 ml of acetonitrile and water (1:1) and kept at -20^{o}C until further analysis.

For inhibition studies, human liver microsomes were incubated with BMS-562086 (1 and 25 μM) for 0, 10, 20 and 30 min in the presence or absence of ketoconazole (5 μM). The concentrations of microsomal proteins, NADPH and phosphate buffer were the same as those used for microsomal incubations described above. For incubations in the presence of ketoconazole, human liver microsomes were pre-incubated for 10 min with the inhibitor before the addition of BMS-562086 and NADPH. The incubations were carried out in microcentrifuge tubes at 37°C for 30 min in a shaking water bath at a final volume of 200 μl. Incubations were stopped by cooling on ice following by addition of 200 μl acetonitrile. The incubation mixture was then centrifuged at 14,000 rpm for 2 min in an Eppendorf model 5417C centrifuge. The supernatants were removed and evaporated to near dryness under a stream of nitrogen. The residues were reconstituted in 50 μl of water and kept at -20°C until analysis. Incubation in the absence of the microsomal protein and incubation in absence of the cofactor NADPH were used as negative controls.

Downloaded from dmd.aspetjournals.org at ASPET Journals on April 19, 2024

DMD Fast Forward. Published on March 1, 2012 as DOI: 10.1124/dmd.111.043596
This article has not been copyedited and formatted. The final version may differ from this version.

Metabolism and Pharmacokinetic Studies in Animals. All the studies were performed according to the *Guide for the Care and Use of Laboratory Animals* (Institute of Laboratory Animal Resources, 1996)

Pharmacokinetic Studies in Rats. One group of male Sprague-Dawley rats (n=3, weight 0.34-0.35 kg) instrumented with single jugular vein cannulas were designated for oral administration; and a second group of male Sprague-Dawley rats (n=3, weight 0.34-0.35 kg) instrumented with dual jugular vein cannulas were designated for intravenous (IV) administration. All rats were fasted for approximately 18 h before use and for 4 h after dosing. Water was provided *ad libitum*. BMS-562086 was administered orally by gavage to three rats at a single dose of 5 mg/kg in 0.5% aqueous methylcellulose. A single IV bolus dose of BMS-562086 was administered to three rats at 1 mg/kg in 20% ethanol in saline via the jugular vein cannula. Blood samples (0.2 ml/time point/animal) were collected via the jugular vein cannula for analysis of BMS-562086 at 0, 0.08 (IV dose only) 0.17 (IV dose only), 0.25, 0.5, 0.75, 1, 2, 4, 8, 12, 24, 48, 72 and 96 h post-dose. Plasma was prepared from the blood samples by centrifuging for 10 min at 1000 g and 5°C.

Metabolism Study in Bile-duct Cannulated (BDC) Rats. BMS-562086 (30 mg/kg) in 0.5% methylcellulose solution was orally administered to BDC male Sprague-Dawley rats (n=3, weight 0.22-0.32 g) by gavage. The animals were individually housed in metabolism cages and fasted overnight before dosing. Urine and bile were collected from the BDC rats at 0-12 h after dosing. Pooled urine and bile samples were prepared by combining equal percentage by weight of urine and bile from all three BDC rats. A 1-ml

Downloaded from dmd.aspetjournals.org at ASPET Journals on April 19, 2024

DMD Fast Forward. Published on March 1, 2012 as DOI: 10.1124/dmd.111.043596
This article has not been copyedited and formatted. The final version may differ from this version.

portion of the pooled urine and bile samples were then centrifuged at 14,000 rpm for 2 min in an Eppendorf model 5417C centrifuge (Eppendrof AG, Hamburg, Germany). Aliquots of the supernatants were analyzed by LC/MS/MS for metabolite identification. Glucuronide hydrolysis was conducted for bile to compare with the profile before the hydrolysis. β-Glucuronide hydrolysis was carried out by incubating 100 μL of pooled bile sample with 70 μL of β-glucuronide enzyme solution (~ 2618 units) in 240 μL of 0.2 M sodium acetate buffer (pH 4.8). The incubation mixture was incubated at 37°C for 16 h in a shaking incubator. The incubation mixture was evaporated to dryness in a Savant SpeedVac SPD2010 Concentrator (Thermo Fisher Scientific, Waltham, MA) at room temperature. The residue was reconstituted in 200 μl acetonitrile/water (3:7, v/v) for LC/MS/MS analysis.

Pharmacokinetic Studies in Dogs. Male beagle dogs (n=3, weight 10.1-12.7kg) were used to conduct the one-way cross-over study in IV and PO dosing. The dogs were fasted for approximately 15 h before use and for 4 h after dosing. Water was provided *ad libitum*. For IV dosing, BMS-562086 was administered as an IV bolus injection through a temporary percutaneous catheter into a saphenous vein at a dose of 1 mg/kg in *N*,*N*-dimethyl-acetamide: propylene glycol: water (1:7:2, v/v/v). One-week washout period was allowed between the IV and PO dosing. For PO dosing, a single dose of BMS-562086 was administered at 5 mg/kg in 0.5% aqueous methylcellulose by oral gavage. Blood samples (2 ml/time point/animal) were collected for analysis of BMS-562086 at 0, 0.08 (IV dose only) 0.17 (IV dose only), 0.25, 0.5, 0.75, 1, 2, 4, 8, 12, 24, 48, 72 and 96 h

Downloaded from dmd.aspetjournals.org at ASPET Journals on April 19, 2024

DMD Fast Forward. Published on March 1, 2012 as DOI: 10.1124/dmd.111.043596
This article has not been copyedited and formatted. The final version may differ from this version.

post-dose. Plasma was prepared from the blood samples by centrifuging for 10 min at 1000 g and 5°C.

Pharmacokinetic Studies in Chimpanzees. Following an overnight fast, BMS-562086 was administered orally to male chimpanzees (n=2, weight 58 and 72 kg) at dose of 1 mg/kg in suspension of 0.5% aqueous methylcellulose and Tang orange juice containing 1% of Tween 80 (1:1, v/v). A single IV dose (over 10 min infusion) of BMS-562086 was administered to one male chimpanzee (weight 60 kg) at 0.5 mg/kg in *N*,*N*-dimethyl-acetamide: propylene glycol: water (1:7:2, v/v/v). Blood samples (0.2 ml/time point/animal) were collected for analysis of BMS-562086 at 0, 0.1 (IV dose only) 0.25 (IV dose only) 0.5 (IV dose only), 1 (IV dose only), 2, 4, 6, 9, 12, 24, 36, 48, 72 and 96 h post-dose. Plasma was prepared from the blood samples by centrifuging for 10 min at 1000 g and 5°C.

Blood to Plasma Ratio in Rats. [^{14}C]BMS-562086 in 0.5% (w/v) aqueous methylcellulose was administered at a target dose level of 5 mg/kg (100 μCi/kg) as a single oral gavage dose to three fasted male Long-Evans rats. Blood samples were collected at 1 h after dosing and pooled together. A portion of the blood was centrifuged for 10 min at 1000 g and 5°C for generation of plasma. Aliquots of blood (approximately 0.05 g) were placed in cones and pads, dried, and combusted. The combustions were performed using a Model 387 Sample Oxidizer (PerkinElmer Life and Analytical Sciences, Meriden, CT). The resulting $^{14}CO_2$ was trapped in Carbo-Sorb E. Following the $^{14}CO_2$ trapping, Permafluor E+ scintillation cocktail (PerkinElmer Life and Analytical Sciences) was added and the mixture was analyzed with a Tri-Carb 3100TR

Downloaded from dmd.aspetjournals.org at ASPET Journals on April 19, 2024

DMD Fast Forward. Published on March 1, 2012 as DOI: 10.1124/dmd.111.043596
This article has not been copyedited and formatted. The final version may differ from this version.

liquid scintillation analyzer (PerkinElmer Life and Analytical Sciences) to determine radioactivity. Aliquots of plasma (0.05 g) were mixed with Emulsifier-Safe scintillation fluid (PerkinElmer Life and Analytical Sciences) and analyzed by Tri-Carb 3100TR liquid scintillation analyzer to determine radioactivity.

LC/MS/MS for Biotransformation Analysis. HPLC analysis was performed on a Shimadzu (Kyoto, Japan) Class VP system equipped with two pumps (model LC-10AD), an autoinjector (model SIL-10AD) and a photodiode array detector (model SPD-M10A. Chromatographic separation was done with a YMC PRO (Waters Corporation, Milford, MA) C18 column (2.0 x 150 mm, 3.0 μ) maintained at 35 ^{o}C in an Eppendorf CH-30 column heater with an Eppendorf TC-45 temperature controller. The solvent system consisted of solvent A, 10 mM ammonium acetate buffer (pH 4.1), and solvent B, acetonitrile/10 mM ammonium acetate buffer (pH 4.1) (90:10, v/v). A linear gradient system was used where solvent B was increased from 0% (0 min) to 100% (60 min) before re-equilibrium. The flow rate was 0.2 ml/min. For the mass spectrometric analysis, the eluant from the HPLC was directed to a LCQ DECA XP ion trap mass spectrometer (Thermo Fisher Scientific) interfaced with an electrospray ionization probe in the positive ion mode. The capillary temperature was kept 275 ^{o}C. The nitrogen gas flow rate, spray current, and voltages were adjusted to give the maximum sensitivity.

Assays of BMS-562086 in Plasma of Rats, Dogs and Chimpanzees. Plasma from pharmacokinetic studies in rats, dogs and chimpanzees was analyzed for unchanged BMS-562086 by a validated LC/MS/MS method. The internal standard used was $^{13}CD_3$-BMS-562086. A 70-μl aliquot of plasma/internal standard mixture was extracted by

Downloaded from dmd.aspetjournals.org at ASPET Journals on April 19, 2024

DMD Fast Forward. Published on March 1, 2012 as DOI: 10.1124/dmd.111.043596
This article has not been copyedited and formatted. The final version may differ from this version.

adding 3 volumes of acetonitrile. Then, the sample was vortexed for 2 min, followed by centrifugation at 14,000 rpm for 2 min in an Eppendorf model 5417C centrifuge. The supernatant was directly analyzed by LC/MS/MS. The HPLC system consisted of two Class VP Shimadzu (Kyoto, Japan) pumps (model LC-10AD) and a PE 200 LC autosampler (PerkinElmer Life and Analytical Sciences, Waltham, MA). A YMC ODS AQ (Waters Corporation) C18 column (2.0 x 50 mm, 5.0 μ) was used with an isocratic solvent system consisting of 20% solvent A, 0.1% formic acid in water, and solvent B, 0.1% formic acid in acetonitrile. The flow rate was 0.3 ml/min. The entire column elute was directly introduced into a Quattro mass spectrometer (Waters Corporation) equipped with an electrospray ionization probe. Analyses were performed in the positive ion mode. Ultra high purity nitrogen was used as the nebulizing gas and desolvation gas. Other parameters were adjusted as needed to achieve maximum sensitivity. Multiple reaction monitoring (MRM) mode was used for detection of BMS-562086 and its internal standard $^{13}CD_3$-BMS-562086. The transition *m/z* 341.02 → *m/z* 285.04 was used for BMS-562086 detection and *m/z* 344.96 → *m/z* 289.04 for $^{13}CD_3$-BMS-562086 detection. Both BMS-562086 and its internal standard $^{13}CD_3$-BMS-562086 were eluted at retention time 1.09 min. The standard curve range for the plasma assay was 1.00 to 1000 ng/ml. Spiked analytical quality control (QC) samples were analyzed along with the study samples for assessment of the accuracy and precision of each analytical run. The QC samples at low, medium and high concentration range of the standard curve were included in the analytical run in a minimum of two replicates. Deviations from the predicted concentrations for at least two-thirds of the QC samples were within ±15% of

Downloaded from dmd.aspetjournals.org at ASPET Journals on April 19, 2024

DMD Fast Forward. Published on March 1, 2012 as DOI: 10.1124/dmd.111.043596
This article has not been copyedited and formatted. The final version may differ from this version.

their nominal values at all concentration levels, with at least one QC sample at each level meeting the acceptance criteria. The LLOQs of the assay were 1.00 ng/ml.

Pharmacokinetic Analysis. Plasma concentration versus time data for BMS-562086 in rats, dogs and Chimpanzees were analyzed by a noncompartmental method using Kinetica ™ 4.2 within the eToolbox (version 2.2) (Thermo Electron Corporation, Philadelphia, PA). The peak concentration (C_{max}), and the time to peak concentration (T_{max}), were obtained from experimental observations. The terminal log-linear phase of the concentration-time curve was identified by least squares linear regression of at least three data points that yield a maximum G-criteria. The half-life ($T_{1/2}$) of the terminal log-linear phase was calculated as ln2/*k*, where *k* is the absolute value of the slope of the terminal log-linear phase, known as the elimination rate constant. The area under the concentration-time curve, AUC(INF), was determined by using the mixed log-linear trapezoidal method. The plasma clearance (CL_p) was calculated as the quotient of dose and AUC(INF) after IV administration. Terminal volume of distribution (V_z) was obtained from dividing the CL_p by the elimination rate constant after IV administration. The absolute oral bioavailability (F) was estimated as the ratio of dose-normalized AUC values following PO and IV doses.

Permeability Analysis. The apparent permeability coefficients (P_{app}, cm/s) through Caco-2 cell monolayers were calculated according to the following equation:

$$P_{app} = \frac{dQ/dt}{A \times C_0}$$

Downloaded from dmd.aspetjournals.org at ASPET Journals on April 19, 2024

DMD Fast Forward. Published on March 1, 2012 as DOI: 10.1124/dmd.111.043596
This article has not been copyedited and formatted. The final version may differ from this version.

where dQ/dt (nmol/s) is the appearance rate of the compound in the receiver compartment (the BL compartment for AP to BL transport); A is the surface area of the monolayer (1 cm^2); and C_0 is the initial concentration of the compound administered in the donor compartment (the AP compartment for AP to BL transport). The appearance rates (dQ/dt) were calculated by plotting the amounts of compound transported to the receiver side *vs* time and determining the slopes of these plots in the linear range. The correlation coefficients (r^2) obtained from the least-squares linear regression analysis were in the range of 0.96-1.00.

Statistical Analysis. Student's t test was used for statistical analysis with a P value of less than 0.05 being considered statistically significant.

Prediction of Human Clearance and Volume of Distribution. The allometric scaling method (Mahmood and Balian, 1996) was used to predict plasma clearance and volume of distribution values in humans. In the simple allometric scaling method, body weights of the animals were used to allometrically scale total plasma clearance values from rats, dogs, and chimpanzees to humans on a log-log scale by using eq. 1, where BW is species body weight (0.34, 11.2, 60, and 70 kg for rats, dogs, chimpanzees and humans, respectively) and *a* and *b* are the coefficient and exponent of the allometric equation, respectively:

$$CL=a*BW^b \quad (1)$$

Downloaded from dmd.aspetjournals.org at ASPET Journals on April 19, 2024

DMD Fast Forward. Published on March 1, 2012 as DOI: 10.1124/dmd.111.043596
This article has not been copyedited and formatted. The final version may differ from this version.

Similarly, allometric scaling was used to estimate human V_z by using both body weight of the animals and the corresponding animal terminal volume of distribution (eq. 2) as follows:

$$V_z = a*BW^b \quad (2)$$

where BW is species body weight (0.34, 11.2, 60, and 70 kg for rats, dogs, chimpanzees and humans, respectively) and *a* and *b* are coefficient and exponent of the allometric equation, respectively.

Prediction of Human Plasma Profiles. The SimCYP population-based ADME simulator (version 10; SimCYP Ltd., Sheffield, UK) was used to perform human plasma profile simulation. The built-in Advanced Dissolution, Absorption and Metabolism (ADAM) model and the minimal Physiologically-Based Pharmacokinetic model were used to construct the final prediction model. A female healthy volunteer population was used for the demographics data as provided in the software. Human plasma profiles were simulated only in women to be consistent with the clinical trial populations defined by pre-clinical safety evaluation (Coric, et al., 2010; Sweetser, et al., 2011). Each dose (oral, once daily for 3 weeks) was simulated with 10 trials and 10 subjects in each trial, which led to a total of 100 simulations.

Downloaded from dmd.aspetjournals.org at ASPET Journals on April 19, 2024

DMD Fast Forward. Published on March 1, 2012 as DOI: 10.1124/dmd.111.043596
This article has not been copyedited and formatted. The final version may differ from this version.

RESULTS

Permeability of BMS-562086 across Caco-2 Cell Monolayers. A permeability coefficient (P_{app}) of 1.7×10^{-5} cm/s was obtained for transport of BMS-562086 in AP to BL direction across Caco-2 cell monolayers. Mannitol, a probe of the caco-2 cell monolayer integrity, had a P_{app} value of 2.1×10^{-7} cm/s for AP to BL in the studies, which was comparable to the reported value in the literature (Zhou et al., 2002).

Serum Protein binding. The extent of protein binding determined in fresh rat, dog and human sera was 93.6, 95.2 and 96.1%, respectively, suggesting a high protein binding for BMS-562086. BMS-562086 did not show concentration-dependent protein binding over the concentration range tested (12.8-38.5 μM). Degradants of BMS-562086 were not detected in the serum samples over the 3-h incubation period, indicating BMS-562086 was stable under the conditions used for protein binding.

Metabolism in Hepatocytes. The biotransformation profiles in mouse, rat, dog, monkey and human hepatocytes after incubation with BMS-562086 are shown in Fig. 1. Metabolites of BMS-562086 were numbered based on their chronologies of identification and did not follow HPLC elution order. HPLC analysis of the positive control samples, 7-EC and 7-HC, showed that the rates of formation of the 7-HC from 7-EC, and formation of 7-HC glucuronide and 7-HC sulfate from 7-HC were comparable to

Downloaded from dmd.aspetjournals.org at ASPET Journals on April 19, 2024

DMD Fast Forward. Published on March 1, 2012 as DOI: 10.1124/dmd.111.043596
This article has not been copyedited and formatted. The final version may differ from this version.

historical data, suggesting competent oxidative and conjugative enzyme activities in hepatocytes (data not shown).

Approximately 75, 68, 61, 83 and 40% of parent disappeared from the incubation of BMS-562086 (25 μM) with mouse, rat, dog, monkey and human hepatocytes for 3 h, respectively. The rate of disappearance of BMS-562086 followed the order of monkeys > mice ≈ rats ≈ dogs > humans. There were a total of 15 metabolites identified. Five oxidative metabolites, DPH-123554, DPH-124921, BMS-572273, M3 and M6 were observed in hepatocytes across all five species. Metabolite M9, an oxidative metabolite that was present in human hepatocytes, was also formed in rat and dog hepatocytes, but not in mouse and monkey hepatocytes. Furthermore, glucuronides (M1, M4, M12 and M13) and sulfate conjugate (M10) were detected in animal species but not in human hepatocytes.

Metabolism in Microsomes. The oxidative metabolites identified in human microsomal incubations, namely, DPH-123554, DPH-124921, BMS-572273, M3, M6 and M9, were also present in the human hepatocyte incubation mixtures and detected at least in mouse microsomal preparation (Table 1). No conjugative metabolites were observed in the microsomal incubations since the microsomes were not fortified with cofactors necessary for conjugation reactions.

A relative formation of BMS-562086 (25 μM) incubated in human liver microsomes for 30 min in the presence or absence of ketoconazole (5 μM) is shown in Fig. 2. DPH-123554 and M6 were the major metabolites identified (measured by UV at 280 nm) in human liver microsomes. The formation of metabolites, DPH-123554, M6 and M9, in

Downloaded from dmd.aspetjournals.org at ASPET Journals on April 19, 2024

DMD Fast Forward. Published on March 1, 2012 as DOI: 10.1124/dmd.111.043596
This article has not been copyedited and formatted. The final version may differ from this version.

human liver microsomes was highly sensitive to ketoconazole inhibition (~ 80% inhibition) (Fig 2). The formation of metabolites DPH-124921, BMS-572273 and M3 was not sensitive to ketoconazole inhibition (Fig 2).

Metabolism in BDC Rats. The biotransformation profiles of 0-12 h pooled urine, 0-12 h pooled bile, and 0-12 h pooled bile hydrolyzed with glucuronidase are shown in Fig. 3. Unchanged BMS-562086 was not detected in either rat urine or bile. A number of oxidative and conjugated metabolites were detected in urine and bile. Five oxidative metabolites (DPH-123554, DPH-124921, BMS-572273, M2 and M3) and two glucuronide metabolites (M1 and M4) were detected in rat urine. Five oxidative metabolites (DPH-123554, BMS-572273, M2, M3 and M6) and three glucuronide metabolites (M1, M4 and M13) were detected in rat bile. Glucuronide metabolites (M4 and M13) were the major metabolites in bile.

The chromatographic pattern of rat bile changed upon incubation with β-glucuronidase. The peaks for M4 and M13 reduced considerably accompanied by the concomitant appearance of the corresponding aglycone peaks M11 and M9, respectively (Panel B and C, Fig. 4). Similarly, the peak for metabolite M1 reduced markedly with the appearance of an aglycone peak M14. The disappearance of metabolites M1, M4 and M13 after hydrolysis by β-glucuronidase confirmed that all three metabolites are glucuronide conjugates. All the metabolites, except M14, that were detected in rat urine and bile, were also observed in rat hepatocyte incubation.

Pharmacokinetics of BMS-562086 in Rats, Dogs and Chimpanzees. The plasma concentration versus time profiles for BMS-582086 after a single IV and PO

Downloaded from dmd.aspetjournals.org at ASPET Journals on April 19, 2024

DMD Fast Forward. Published on March 1, 2012 as DOI: 10.1124/dmd.111.043596
This article has not been copyedited and formatted. The final version may differ from this version.

administration to rats, dogs and chimpanzees are shown in Fig. 4. The pharmacokinetic parameters of BMS-562086 following the IV and PO administration to rats, dogs and chimpanzees are summarized in Table 2. After the IV bolus dose, the plasma BMS-562086 concentrations exhibited a multi-exponential decline in rats, dogs and chimpanzees. The plasma clearance (CL_p) of BMS-562086 was higher in rats (17.9 ml/min/kg) and dogs (11.6 ml/min/kg) than in chimpanzees (2.0 ml/min/kg). Assuming the value of plasma clearance CL_p of BMS-562086 approximates the value of blood clearance CL_b in these three species, BMS-562086 has an estimated hepatic extraction ratio of 0.32, 0.38 and 0.08 in rats, dogs and chimpanzees, respectively (calculated by dividing CL_p by respective hepatic blood flow, 55.2, 30.9 and 25.5 ml/min/kg for rats, dogs and chimpanzees) (Davies and Morris, 1993; Wong et al., 2004). The assumption that CL_b is equal to CL_p is reasonable at least in rats, where the blood to plasma concentration ratio of BMS-562086-equivalent radioactivity was 0.95 at 1 h post-dose. The average terminal volume of distribution (V_z) of BMS-582086 in the rats, dogs and chimpanzee was 14.9, 28.2 and 4.2 L/kg, respectively. The V_z was approximately 22, 47 and 7-fold greater than total body water for rats (0.67 L/kg), dogs (0.60 L/kg) and chimpanzees (0.60 L/kg), respectively, indicating extensive extravascular distribution. The terminal plasma elimination half-lives ($T_{1/2}$) ranged from 13 to 43 h in rats, dogs and chimpanzees. Following oral administration, peak plasma concentrations (T_{max}) were achieved in less than 2 h for all three species, indicating a rapid oral absorption. BMS-

Downloaded from dmd.aspetjournals.org at ASPET Journals on April 19, 2024

DMD Fast Forward. Published on March 1, 2012 as DOI: 10.1124/dmd.111.043596
This article has not been copyedited and formatted. The final version may differ from this version.

562086 was orally bioavailable in rats, dogs and chimpanzees, with an absolute oral bioavailability of 40.1 %, 58.8, and 58.5%, respectively.

LC/MS/MS Characterization of the Metabolites. The LC/MS/MS characterization of BMS-562086 and its metabolites identified in mouse, rat, dog, monkey and human microsomes and hepatocytes, and in BDC rats are shown in Table 1 and Fig. 7. The mass spectral fragmentation patterns for BMS-562086 and its metabolites are illustrated on the structures listed at the top of Table 1. The identification for BMS-562086, DPH-123554, DPH-124921 and BMS-572273 was based on its MS/MS fragmentation and comparison of its chromatographic retention times with the reference standards. The structures of the other metabolites were proposed by their LC/MS/MS fragmentation patterns.

BMS-562086 showed a protonated molecular ion at *m/z* 341. The base peak in the product ion spectrum was observed at *m/z* 285, consistent with a neutral loss of a butylene molecule (C_4H_8, 56 Da). A loss of a molecule of C_4H_9NHCN (98 Da) from the protonated molecular ion gave rise to a product ion at *m/z* 243.

DPH-123554, formed by *O*-demethylation of BMS-562086, had a protonated molecular ion at *m/z* 327. Its product ion spectrum yielded one abundant ion at *m/z* 271 and one minor ion at *m/z* 229, attributable to a neutral loss of a butylene molecule (C_4H_8) and a C_4H_8NHCN molecule from the protonated molecular ion, respectively.

DPH-124921, formed by *N*-dealkylation of BMS-562086, showed a protonated molecular ion at *m/z* 285. The product ion spectrum obtained from *m/z* 285 exhibited two abundant ions at *m/z* 270, a loss of $\bullet CH_3$; and *m/z* 243, a loss of NH_2CN.

Downloaded from dmd.aspetjournals.org at ASPET Journals on April 19, 2024

DMD Fast Forward. Published on March 1, 2012 as DOI: 10.1124/dmd.111.043596
This article has not been copyedited and formatted. The final version may differ from this version.

BMS-572273, formed by *N*-dealkylation followed by hydrolysis of BMS-562086, had a protonated molecular ion at *m/z* 286, which is 1 Da higher than that of DPH-124921. The product ion spectrum of *m/z* 286 showed a loss of HOCN, resulting in a fragment ion at *m/z* 243.

Metabolite M1 was identified as a glucuronide conjugate of the oxidized and *N*-dealkylated product of BMS-562086, namely, a glucuronide conjugate of the oxidized product of DPH-124921. The protonated molecular ion of metabolite M1 was observed at *m/z* 477. Fragmentation of the molecular ion at *m/z* 477 yielded a major ion at *m/z* 301, attributable to a neutral loss of 176 Da from the protonated molecular ion, indicating that M1 was a glucuronide conjugate. The ion at *m/z* 301 is 16 Da higher than the protonated molecular ion of DPH-124921 (*m/z* 285), suggesting that the ion at *m/z* 301 structurally represented an oxidized product of DPH-124921. An additional loss of a H_2O molecule from the ion at *m/z* 301 generated a minor ion at *m/z* 283 in the product ion spectrum.

Metabolite M2 was identified as a product of bis-oxidation followed by dehydrogenation of BMS-562086. The oxidation positions were determined to have occurred on the *N*-alkyl side chain of the molecule. The protonated molecular ion of metabolite M2 was observed at *m/z* 371, which is 30 Da higher than that of BMS-562086. Upon MS^2 analysis, M2 showed a product ion at *m/z* 243, the same fragment ion as that of BMS-562086, DPH-124921 and BMS-572273, suggesting that they all share the same core aromatic ring structure. Therefore, the oxidation positions were assigned on the *N*-alkyl side chain of the molecule.

Downloaded from dmd.aspetjournals.org at ASPET Journals on April 19, 2024

DMD Fast Forward. Published on March 1, 2012 as DOI: 10.1124/dmd.111.043596
This article has not been copyedited and formatted. The final version may differ from this version.

Metabolite M3 was an oxidation and *O*-demethylation product of BMS-562086 (the oxidized product of DPH-123554) with the oxidation site occurring on the *N*-alkyl side chain of the molecule. The protonated molecular ion of metabolite M3 was observed at *m/z* 343, which is 16 Da higher than that of DPH-123554 (*O*-demethylation of BMS-562086). Two prominent product ions were observed in the product ion spectrum upon fragmentation of the molecular ion at *m/z* 343. The presence of a product ion at *m/z* 229 which was also a product ion of DPH-123554, suggested that the oxidation has occurred on the *N*-alkyl side chain of the molecule. The base peak in the product ion spectrum, *m/z* 272, was consistent with the replacement of the *N*-alkyl side chain of the molecular ion with an -OH group.

Metabolite M4 was determined to be a glucuronide conjugate of the bis-oxidation product of BMS-562086 (a glucuronide conjugate of metabolite M11). The protonated molecular ion of M4 was observed at *m/z* 549. The base peak in the product ion spectrum, *m/z* 373, was generated by a neutral loss of 176 Da, indicating that M4 is a glucuronide conjugate. The MS^3 spectrum of M4 (*m/z* 549→*m/z* 373→) contained product ions at *m/z* 355, 302 and 259, which are consistent with a bis-oxidation product of BMS-562086 (metabolite M11, to be characterized below), supporting the assignment of M4 as a glucuronide conjugate of the bis-oxidation product of BMS-562086.

Metabolites M5, M6 and M7 were positional isomers, each identified as the product of bis-oxidation coupled with dehydrogenation of DPH-123554 (the *O*-demethylated BMS-562086). The oxidation position was tentatively assigned to occur on one of the three methyl groups on the pyrazolotriazine ring moiety. M5, M6 and M7 were

Downloaded from dmd.aspetjournals.org at ASPET Journals on April 19, 2024

DMD Fast Forward. Published on March 1, 2012 as DOI: 10.1124/dmd.111.043596
This article has not been copyedited and formatted. The final version may differ from this version.

chromatographically adjacent to each other and all had a protonated molecular ion at *m/z* 357, which is 30 Da higher than that of DPH-123554 (or 16 Da higher than that of the parent). The spectrum of molecular ion at *m/z* 357 for all three metabolites showed fragment ions at *m/z* 329, 286 and 243. The ion at *m/z* 329 was the characteristic ion, produced by a loss of CO (28 Da), suggesting the presence of a -COOH group in the structure (formed by bis-oxidation coupled with dehydrogenation). The product ion at *m/z* 243 was likely produced by a loss of $C_5H_9N_2$• (97 Da) and •OH (17 Da) from the protonated molecular ion. The product ion at *m/z* 286 was proposed to arise from a loss of C_5H_8NH, a molecule derived from the *N*-alkyl side chain.

Metabolites M8 and M9 were positional isomers of mono-hydroxylation products of BMS-562086. The hydroxylation positions were determined to occur on the *N*-alkyl side chain. Both metabolites showed a protonated molecular ion at *m/z* 357, 16 Da higher than that of the parent. The major product ions at *m/z* 286 and 243, the same fragment ions as these of M2, suggesting that M2, M8 and M9 have the same core aromatic ring structure. Since metabolites M8 and M9 fragmented in a similar pattern, the exact oxidation position could not be further established.

Metabolite M10 was identified as a sulfate conjugate of the hydroxylated BMS-562086. M10 had a protonated molecular ion at *m/z* 437. Fragmentation of *m/z* 437 yielded a predominant ion at m/z 357, attributable to a neutral loss of 80 Da from the molecular ion which indicated that metabolite M10 is a sulfate conjugate. MS^3 analysis of *m/z* 357 (*m/z* 437→*m/z* 357→), produced fragments at *m/z* 301 and 283, consistent with a neutral loss of a butylene molecule (C_4H_8, 56 Da) and a further loss of H_2O from the protonated

Downloaded from dmd.aspetjournals.org at ASPET Journals on April 19, 2024

DMD Fast Forward. Published on March 1, 2012 as DOI: 10.1124/dmd.111.043596
This article has not been copyedited and formatted. The final version may differ from this version.

molecule of hydroxylated BMS-562086, respectively. The fact that a butylene molecule (C_4H_8) was observed (*m/z* 357→*m/z* 301), as seen in the fragmentation of protonated molecular ion of BMS-562086 (*m/z* 341→*m/z* 285, a loss of 56 Da), suggested that the hydroxylation position was not on the *N*-alkyl side chain.

Metabolite M11, the aglycone of metabolite M4, was identified as a bis-oxidation product of BMS-562086. M11 had a protonated molecular ion at *m/z* 373 (32 Da higher than that of BMS-562086) and major MS^2 product ions at *m/z* 355, 302 and 259. The product ion at *m/z* 355 was consistent with a loss of H_2O from the protonated molecular ion at *m/z* 373. The product ion at *m/z* 302 resulted from a loss of the *N*-alkyl side chain followed by an addition of hydroxyl group. A loss of a molecule of $(HO)C_4H_9NHCN$ (98 Da) from the protonated molecular ion gave rise to a product ion at *m/z* 259.

Metabolite M12 was identified as a glucuronide conjugate of an oxidation product of BMS-562086. Metabolite M12 had a protonated molecular ion at *m/z* 533, which is 176 Da higher than that of the oxidation product of BMS-562086. MS^3 analysis of *m/z* 357 (*m/z* 533→*m/z* 357→), produced fragments at *m/z* 301, consistent with a neutral loss of a butylene molecule (C_4H_8, 56 Da). The fact that a butylene molecule (C_4H_8) was observed (*m/z* 357→*m/z* 301), as seen in the fragmentation of protonated molecular ion of BMS-562086 (*m/z* 341→*m/z* 285, a loss of 56 Da), suggested that the oxidation position was not on the *N*-alkyl side chain.

Metabolite M13 was identified as the glucuronide conjugate of M9, an oxidation product of BMS-562086. The protonated molecular ion of metabolite M13 was observed at m/z

Downloaded from dmd.aspetjournals.org at ASPET Journals on April 19, 2024

DMD Fast Forward. Published on March 1, 2012 as DOI: 10.1124/dmd.111.043596
This article has not been copyedited and formatted. The final version may differ from this version.

533. Fragmentation on m/z 533 gave an ion at m/z 357, attributable to a neutral loss of 176 Da from the molecular ion, indicating that M13 is a glucuronide conjugate. The MS^3 analysis of m/z 357 (*m/z* 533→*m/z* 357→), produced fragments at m/z 243 and 286, a fragmentation pattern similar to that of M9. These data, along with the fact that the reduced peak for M13 after hydrolysis of rat bile by β-glucuronidase was accompanied by the concomitant appearance of the peak for M9 (Panel B and C, Fig. 4) suggested that Metabolite M13 was the glucuronide conjugate of M9.

Metabolite M14, the aglycone of M1, was identified as an oxidized and *N*-dealkylated product of BMS-562086. Metabolite M14 was only observed in rat bile after hydrolysis by β-glucuronidase. Its fragmentation pattern has been assigned earlier, along these of M1.

Prediction of Human Pharmacokinetic Parameters. Human plasma CL and V_z values predicted for BMS-562086 by allometric scaling method are shown in Fig. 5. The human plasma CL and V_z values predicted for BMS-562086 were 2.97 ml/min/kg and 7.79 L/kg (208 ml/min and 545 L for a 70-kg human), respectively. The coefficient (*a*) and exponent (*b*) of the allometric equation used for the estimation of CL were 14.80 and 0.62. The coefficient (*a*) and exponent (*b*) of the allometric equation used for the estimation of V_z was 16.74 and 0.82. The correlation coefficients (R^2) for the estimation of CL and V_z were 0.88 and 0.87, respectively.

Prediction of Human Plasma Profiles. The human projected plasma concentration-time profile of BMS-562086 after once daily oral dose of 100 mg of BMS-562086 for

Downloaded from dmd.aspetjournals.org at ASPET Journals on April 19, 2024

DMD Fast Forward. Published on March 1, 2012 as DOI: 10.1124/dmd.111.043596
This article has not been copyedited and formatted. The final version may differ from this version.

three weeks was simulated using SymCYP population-based ADME simulator (Fig. 6). The simulated plasma concentration-time profile indicated that the steady-state plasma concentration was achieved by the end of week one, with the total mean plasma concentration values in the range of 925-1300 nM (trough to peak). The individual trials suggested the variability was likely moderate, with trough-peak values in the range of 725-1530 nM in the female healthy volunteer population.

Downloaded from dmd.aspetjournals.org at ASPET Journals on April 19, 2024

DMD Fast Forward. Published on March 1, 2012 as DOI: 10.1124/dmd.111.043596
This article has not been copyedited and formatted. The final version may differ from this version.

DISCUSSION

Metabolism. The primary biotransformation pathways found for BMS-562086 in both liver microsomal and hepatocyte preparations and in rats included: (a) *O*-demethylation to DPH-123554, (b) hydroxylation at the *N*-alkyl side chain to metabolites M8 and M9, and (c) *N*-dealkylation to DPH-124921. BMS-562086 was further metabolized via multiple pathways including oxidation, glucuronidation and sulfation of the oxidative products, and combination of the above pathways. The proposed biotransformation pathways for BMS-562086 are shown in Fig. 7. Since the primary biotransformation pathways are oxidative in nature, cytochrome P450 enzymes play a critical role in the overall metabolic clearance of BMS-562086. Furthermore, the absence of direct conjugative metabolites suggests a limited role for the conjugative enzymes in overall metabolic clearance. The formation of the two prominent primary metabolites, DPH-123554 and M9, was highly sensitive to ketoconazole inhibition in human liver microsomes; indicative of the significant involvement of CYP3A4/5 in the BMS-562086 metabolic elimination. The formation of the primary metabolite DPH-124921 was not sensitive to ketoconazole inhibition, suggesting the metabolic elimination of BMS-562086 was not entirely dependent on CYP3A4/5. Taken together, the metabolic clearance of BMS-562086 was mediated by multiple CYP P450s including CYP3A4/5. Even though the fractions metabolized through these pathways are not known, the involvement of multiple enzymes in the overall metabolic clearance should reduce the potential for drug-drug interaction through modulation of a single elimination pathway.

Downloaded from dmd.aspetjournals.org at ASPET Journals on April 19, 2024

DMD Fast Forward. Published on March 1, 2012 as DOI: 10.1124/dmd.111.043596
This article has not been copyedited and formatted. The final version may differ from this version.

No unique human metabolites were detected in human liver microsomes and hepatocytes. The in vitro metabolic profiles were qualitatively similar across mice, rats, dogs and humans. The similarity among biotransformation profiles across the five species for BMS-562086 helps in justifying the selection of the animal species to be employed for toxicological evaluation. DPH-123554 and DPH-124921 were identified as the prominent metabolites of BMS-562086 in both liver microsomal and hepatocyte preparations and in vivo in rats. Both metabolites were inactive towards rat CRF binding with IC_{50} values > 1000 nM, suggesting that they are unlikely to contribute to the pharmacology of BMS-562086. BMS-562086 was significantly metabolized in hepatocytes in all species. BMS-562086 was not detected in rat urine and bile, indicating the absorbed compound was metabolized completely prior to elimination in rats. BMS-562086-derived metabolites were found in both urine and bile of rats, suggesting both urinary and biliary pathways were involved in the elimination of the metabolites in rats (Fig. 3). Because of the significant contribution of metabolism to its overall elimination, an evaluation of the impact on pharmacokinetics of BMS-562086 in subjects with hepatic impairment is warranted in future clinical studies. On the other hand, pharmacokinetics of BMS-562086 in subjects with renal impairment is not expected to be altered due to the lack of contribution of renal excretion to its total clearance.

ADME studies in preclinical species and humans with radiolabeled material are typically performed to provide quantitative understanding of the role of each metabolic pathway in the elimination of a compound. However, earlier studies in discovery are conducted with non-radiolabeled compound. Nonetheless, the results of the metabolic in vitro and in

Downloaded from dmd.aspetjournals.org at ASPET Journals on April 19, 2024

DMD Fast Forward. Published on March 1, 2012 as DOI: 10.1124/dmd.111.043596
This article has not been copyedited and formatted. The final version may differ from this version.

vivo investigation provide key information for the appropriate placement of the radiolabel. If the label is incorporated in a metabolically labile moiety of the molecule, there is a chance that it may be liberated through metabolism. If the labile moiety is similar to an endogenous compound, it may get incorporated into cellular components. These events could lead to poor recovery of radioactivity and could pose safety concern as there could be extended tissue exposure to radioactivity. The metabolites derived from BMS-562086 were produced by modifications mainly of the side-chain groups, whereas the core pyrazolotriazine ring structure was intact in all of the metabolites indentified. Therefore, introducing the radiolabel on the pyrazolotriazine ring rather than the side-chains would ensure a good recovery of radioactivity and would not lead to endogenous incorporation of the label.

Absorption. Permeability of BMS-562086 across Caco-2 cell monolayers in the absorption direction was high and comparable to the value for compounds that exhibit good absorption in humans (Zhou, et al., 2002). Permeability of BMS-562086 in the secretory direction was not done in this study. Thus, it is not known whether or not BMS-562086 is a substrate of efflux transporter such as P-glycoprotein based on Caco-2 results. However, preliminary work with isolated rat duodenum, jejunum, ileum and colon muscle layers demonstrated that the BL-to-AP permeability was not higher than the AP-to-BL permeability, suggesting that BMS-562086 may not be a substrate of efflux transporters (data not shown). The high permeability determined for BMS-562086 by the Caco-2 experiments was consistent with its good oral bioavailability observed in animals. The absolute oral bioavailability of BMS-562086 achieved 40.1%, 58.8% and 58.5% in

Downloaded from dmd.aspetjournals.org at ASPET Journals on April 19, 2024

DMD Fast Forward. Published on March 1, 2012 as DOI: 10.1124/dmd.111.043596
This article has not been copyedited and formatted. The final version may differ from this version.

rats, dogs and chimpanzees, respectively. Both high permeability and an extensive metabolism profile of BMS-562086 agrees well with the observation made by Benet who recognized that the major route of elimination for highly permeable drugs was mainly through metabolism (Benet, 2010).

Prediction of Human Pharmacokinetics. The extraction ratio characterized BMS-562086 as a moderate hepatic clearance compound in rats and dogs, but a low hepatic clearance compound in chimpanzees. The chimpanzees are the closest living relatives to humans and are viewed as a valuable surrogate model for human ADME (Wong et al., 2004). The chimpanzee was chosen as a pharmacokinetic model in this study to aid in the selection of drug candidates for clinical development.

The plasma clearance of BMS-562086 was predicted to be 2.97 ml/min/kg for a 70-kg human. The predicted plasma clearance represented a hepatic extraction ratio of 0.14 if compared to a hepatic blood flow of 20.7 ml/min/kg in humans and assumed that the plasma clearance CL_p had a similar value to blood clearance CL_b. The predicted V_z value in humans was 545 L (7.79 L/kg) for a 70-kg human, a value approximately 13-fold greater than that of the total body water (42 L). Thus, the human CL and V_z values predicted by the allometric scaling method suggested low plasma clearance and significant extravascular distribution for BMS-562086 in humans. The elimination $T_{1/2}$ was expected to be long in humans. The allometric equation for clearance prediction gave an exponent of 0.62 which was between the lower and upper limit values of 0.55 and 0.70 to indicate a reasonable good clearance prediction (Mahmood and Balian, 1996). This prediction was validated in the single ascending dose (SAD) studies where

Downloaded from dmd.aspetjournals.org at ASPET Journals on April 19, 2024

DMD Fast Forward. Published on March 1, 2012 as DOI: 10.1124/dmd.111.043596
This article has not been copyedited and formatted. The final version may differ from this version.

the predicted human clearance of BMS-562086 matched the observed human clearance (data not shown).The human plasma concentration-time profiles of BMS-562086 were simulated using the SymCYP population-based ADME simulator (Fig. 6). The simulation results suggested BMS-562086 was able to achieve the mean trough concentration values above the projected human efficacious concentration of >500 nM after a 100 mg daily oral dose (Coric, et al., 2010). Furthermore, the mean trough concentration values for each individual trial were all above 500 nM, suggesting that the targeted concentration would be achieved in a majority of subjects rather than just an "average one" (Cubitt et al., 2011). The simulated steady-state concentrations (925-1300 nM) were within 2-fold of the observed clinical serum concentrations of BMS-562086 at weeks 4-6, where the average mean concentration was 1630 nM after a 100 mg daily oral administration to patients with generalized anxiety disorder (Coric, et al., 2010; Sweetser, et al., 2011).

In summary, BMS-562086 exhibited favorable ADME and pharmacokinetic properties making it a suitable candidate for further development. BMS-562086 was rapidly absorbed in rats, dogs and chimpanzees with good oral bioavailability. Metabolism studies suggested that multiple pathways, including CYP3A4/5 dependent and non-dependent reactions, mediated the metabolic clearance of BMS-562086. BMS-562086 was metabolized completely prior to elimination in rats. Both renal and biliary excretion played a role in the elimination of BMS-562086 metabolites. A 100 mg daily dose was predicted to be the minimum daily dose to provide sufficient drug exposure to exhibit efficacy. The compound was therefore chosen to advance to clinical development as a

Downloaded from dmd.aspetjournals.org at ASPET Journals on April 19, 2024

DMD Fast Forward. Published on March 1, 2012 as DOI: 10.1124/dmd.111.043596
This article has not been copyedited and formatted. The final version may differ from this version.

potentially effective agent intended for the oral treatment of generalized anxiety disorder and IBS (Coric, et al., 2010; Sweetser, et al., 2011).

Downloaded from dmd.aspetjournals.org at ASPET Journals on April 19, 2024

DMD Fast Forward. Published on March 1, 2012 as DOI: 10.1124/dmd.111.043596
This article has not been copyedited and formatted. The final version may differ from this version.

Authorship Contributions

Participated in research design: Zhou, Dockens, Iyer, and Grossman

Conducted experiments: Zhou and Liu-Kreyche

Contributed new reagents or analytical tools: Zhou and Liu-Kreyche

Performed data analysis: Zhou and Dockens

Write or contributed to the writing of the manuscript: Zhou, Dockens and Iyer

Downloaded from dmd.aspetjournals.org at ASPET Journals on April 19, 2024

DMD Fast Forward. Published on March 1, 2012 as DOI: 10.1124/dmd.111.043596
This article has not been copyedited and formatted. The final version may differ from this version.

References

Benet LZ (2010) Predicting drug disposition via application of a Biopharmaceutics Drug Disposition Classification System. *Basic Clin Pharmacol Toxicol* **106**:162-7.

Coric V, Feldman HH, Oren DA, Shekhar A, Pultz J, Dockens RC, Wu X, Gentile KA, Huang SP, Emison E, Delmonte T, D'Souza BB, Zimbroff DL, Grebb JA, Goddard AW, Stock EG (2010) Multicenter, randomized, double-blind, active comparator and placebo-controlled trial of a corticotropin-releasing factor receptor-1antagonist in generalized anxiety disorder. *Depress Anxiety*. **27**:417-25.

Cubitt HE, Yeo KR, Howgate EM, Rostami-Hodjegan A, Barter ZE (2011) Sources of interindividual variability in IVIVE of clearance: an investigation into the prediction of benzodiazepine clearance using a mechanistic population-based pharmacokinetic model. *Xenobiotica*. **41**:623-38.

Davies B, Morris T (1993) Physiological parameters in laboratory animals and humans. *Pharm Res* **10**:1093-5.

Fukudo S, Nomura T, Hongo M (1998) Impact of corticotropin-releasing hormone on gastrointestinal motility and adrenocorticotropic hormone in normal controls and patients with irritable bowel syndrome. *Gut* **42**:845-9.

Gilligan PJ, Clarke T, He L, Lelas S, Li YW, Heman K, Fitzgerald L, Miller K, Zhang G, Marshall A, Krause C, McElroy JF, Ward K, Zeller K, Wong H, Bai S, Saye J, Grossman S, Zaczek R, Arneric SP, Hartig P, Robertson D, Trainor G (2009) Synthesis and structure-activity relationships of 8-(pyrid-3-yl)pyrazolo[1,5-a]-1,3,5-triazines: potent,

Downloaded from dmd.aspetjournals.org at ASPET Journals on April 19, 2024

DMD Fast Forward. Published on March 1, 2012 as DOI: 10.1124/dmd.111.043596
This article has not been copyedited and formatted. The final version may differ from this version.

orally bioavailable corticotropin releasing factor receptor-1 (CRF1) antagonists. *J Med Chem* **52**:3084-92.

Humphreys WG and Unger SE (2006) Safety assessment of drug metabolites: Characterization of chemically stable metabolites. *Chem Res Toxicol* **19**:1564-9.

Institute of Laboratory Animal Resources (1996) *Guide for the Care and Use of Laboratory Animals*, 7th ed. Institute of Laboratory Animal Resources, Commission on Life Sciences, National Research Council, Washington DC.

Iyer R and Zhang D (2008) Role of drug metabolism in drug development, in *Drug Metabolism in Drug Design and Development* (Zhang D, Zhu M and Humphreys WG eds) pp 261-285, John Wiley & Sons, New York.

Mahmood I and Balian JD (1996) Interspecies scaling: predicting clearance of drugs in humans. Three different approaches. *Xenobiotica* **26**:887–95.

Owens MJ and Nemeroff CB(1991) Physiology and pharmacology of corticotropin-releasing factor. *Pharmacol Rev* **43**:425-73.

Smagin GN, Dunn AJ (2000) The role of CRF receptor subtypes in stress-induced behavioural responses. *Eur J Pharmacol* **405**:199-206.

Sweetser S, Camilleri M, Linker Nord SJ, Burton DD, Castenada L, Croop R, Tong G, Dockens R, Zinsmeister AR (2009) Do corticotropin releasing factor-1 receptors

Downloaded from dmd.aspetjournals.org at ASPET Journals on April 19, 2024

DMD Fast Forward. Published on March 1, 2012 as DOI: 10.1124/dmd.111.043596
This article has not been copyedited and formatted. The final version may differ from this version.

influence colonic transit and bowel function in women with irritable bowel syndrome? *Am J Physiol Gastrointest Liver Physiol* **296**:G1299-306.

Wong H, Grossman SJ, Bai SA, Diamond S, Wright MR, Grace JE Jr, Qian M, He K, Yeleswaram K, Christ DD (2004) The chimpanzee (Pan troglodytes) as a pharmacokinetic model for selection of drug candidates: model characterization and application. *Drug Metab Dispos* **32**:1359-69.

Zhou L, Lee K, Thakker DR, Boykin DW, Tidwell RR, Hall JE (2002) Enhanced permeability of the antimicrobial agent 2,5-bis(4-amidinophenyl)furan across Caco-2 cell monolayers via its methylamidoxime prodrug. *Pharm Res* **19**:1689-95.

Downloaded from dmd.aspetjournals.org at ASPET Journals on April 19, 2024

DMD Fast Forward. Published on March 1, 2012 as DOI: 10.1124/dmd.111.043596
This article has not been copyedited and formatted. The final version may differ from this version.

Legend for Figures

Fig. 1 Biotransformation profiles in mouse, rat, dog, monkey and human hepatocytes after incubation of 25 μM of BMS-562086 for 3 h.

Fig. 2 A relative formation of metabolites of BMS-562086 (25 μM) in the presence (filled symbol) or absence (open symbol) of ketoconazole (5 μM) in human liver microsomes after 30-min incubation.

Fig. 3 The biotransformation profiles of 0-12 h pooled urine (A), 0-12 h pooled bile (B), and 0-12 h pooled bile hydrolyzed with glucuronidase (C) after single oral administration of 30 mg/kg of BMS-562086 to rats (n=3).

Fig. 4 Plasma concentration versus time profiles for BMS-562086 in rats, dogs and chimpanzees following a single IV and PO administration. Plasma BMS-562086 was measured by HPLC/MS/MS. The inserts show the plasma concentration profiles at 1-4 h.

Fig. 5 Prediction of Plasma clearance (left panel) and steady-state volume of distribution (right panel) of BMS-562086 in humans by interspecies allometric scaling

Fig. 6 Human projected plasma concentration-time profiles of BMS-562086 after once daily oral dose of 100 mg of BMS-562086 for three weeks were simulated using SymCYP population-based ADME simulator. Simulations were performed with 10 virtual trials and 10 subjects in each trial, which led to a total of 100 virtual trials.

Fig. 7 Proposed biotransformation pathways for BMS-562086. The proposed MS/MS fragmentation is marked with dashed lines. The mjor fragment ions are also denoted on the structures.

Downloaded from dmd.aspetjournals.org at ASPET Journals on April 19, 2024

DMD Fast Forward. Published on March 1, 2012 as DOI: 10.1124/dmd.111.043596
This article has not been copyedited and formatted. The final version may differ from this version.

Tables

TABLE 1

LC/MS/MS characterization of BMS-562086 and its metabolites identified in mouse, rat, dog, monkey and human microsomes and hepatocytes, and in bile-duct cannulated rats

Downloaded from dmd.aspetjournals.org at ASPET Journals on April 19, 2024

DMD Fast Forward. Published on March 1, 2012 as DOI: 10.1124/dmd.111.043596
This article has not been copyedited and formatted. The final version may differ from this version.

Metabolite	*HPLC RT (min)*	*MH^+*	*Major MS^2 (MS^3) Fragment Ions*	*Species/Matrix*		
				Hepatocytes	Microsomes	BDC Rat
BMS-562086 (Parent)	52.2	341	285, 243	Mouse, Rat, Dog, Monkey, Human	Mouse, Rat, Dog, Monkey, Human	–
DPH-123554	32.1	327	271, 229	Mouse, Rat, Dog, Monkey, Human	Mouse, Rat, Dog, Monkey, Human	Urine, Bile
DPH-124921	28.5	285	270, 243	Mouse, Rat, Dog, Monkey, Human	Mouse, Rat, Dog, Monkey, Human	Urine
BMS-572273	25.6	286	243	Mouse, Rat, Dog, Monkey, Human	Mouse, Rat, Dog, Monkey, Human	Urine, Bile
M1	16.2	477	301, 283	Rat	N/A	Urine, Bile
M2	34.5	371	311, 286, 243	Mouse, Rat, Monkey	_	Urine, Bile
M3	20.1	343	272, 229	Mouse, Rat, Dog, Monkey, Human	Mouse, Human	Urine, Bile
M4	23.6	549	373, (355, 302, 259)*	Rat, Monkey	N/A	Urine, Bile
M5	36.0	357	329, 286, 243	Mouse, Rat, Monkey	Mouse, Rat, dog, Monkey	–
M6	38.1	357	329, 286, 243	Mouse, Rat, Dog, Monkey, Human	Mouse, Rat, Dog, Monkey, Human	Bile
M7	38.8	357	329, 286, 243	Mouse, Rat, Monkey	Mouse, Rat, dog, Monkey	–
M8	44.7	357	286, 243	Monkey	Monkey	_
M9	45.6	357	286, 243	Rat, Dog, Human	Mouse, Rat, Dog, Monkey Human	Bile***
M10	47.7	437	357, (301, 283)**	Dog	N/A	_
M11	31.2	373	355, 302, 259	Rat	Rat, Monkey	Bile***
M12	33.2	533	357, (301) *	Dog	N/A	_
M13	30.2	533	357, (243, 286)*	Rat	N/A	Bile
M14	22.8	301	283	_	_	Bile***

* *MS^3 fragment ions [$MH^+ \rightarrow m/z\ 357 \rightarrow$]*

Downloaded from dmd.aspetjournals.org at ASPET Journals on April 19, 2024

DMD Fast Forward. Published on March 1, 2012 as DOI: 10.1124/dmd.111.043596
This article has not been copyedited and formatted. The final version may differ from this version.

** *MS^3 fragment ions [$MH^+ \rightarrow$m/z 373$\rightarrow$]*

*** *Observed only after hydrolysis by β-glucuronidase*

Downloaded from dmd.aspetjournals.org at ASPET Journals on April 19, 2024

DMD Fast Forward. Published on March 1, 2012 as DOI: 10.1124/dmd.111.043596
This article has not been copyedited and formatted. The final version may differ from this version.

TABLE 2

Pharmacokinetic parameters (mean ± SD) of BMS-562086 in rats, dogs and chimpanzees.

Species	Route	Dose (mg/kg)	Cmax (nM)	Tmax (h)	AUC(INF) (nM·h)	T 1/2 (h)	CLp (ml/min/kg)	Vz (l/kg)	F (%)
Rat	IV	1	–	–	2900±912	13.5±3.1	17.9±4.8	14.9±1.0	–
	PO	5	1261±552	0.75 * (0.5, 0.75)	5815±1307	13.81.8	–	–	40.1
Dog	IV	1	–	–	4296±789	43.9±8.2	11.6±2.0	28.2±5.6	–
	PO	5	1798±516	0.75 * (0.25, 1.0)	13043±6369	46.7±5.1	–	–	58.8±18
Chimp.**	IV	0.5	–		11900	30	2.0	4.2	
	PO	1	1070 (840, 1300)	2 (2, 2)	13900 (11700,16100)	26 (26, 26)	–		58.5 (49, 68)

** Median (minimum, maximum)*

*** SD was not obtained since only two animals were used for oral administration and one animal for IV administration. Pharmacokinetic parameters were reported as mean (minimum, maximum) for oral administration.*

Downloaded from dmd.aspetjournals.org at ASPET Journals on April 19, 2024

Fig. 1

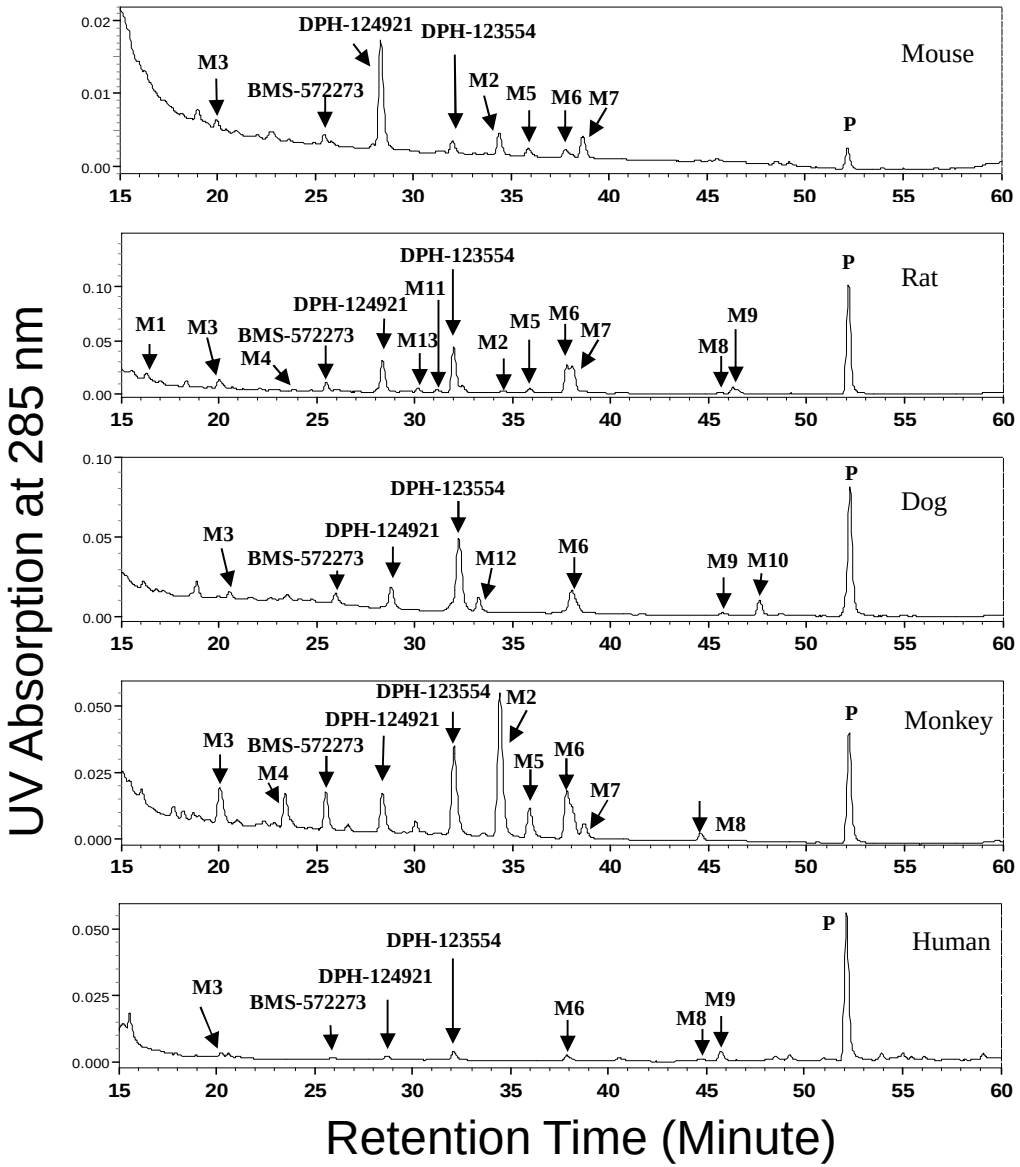

DMD Fast Forward. Published on March 1, 2012 as DOI: 10.1124/dmd.111.043596
This article has not been copyedited and formatted. The final version may differ from this version.

Downloaded from dmd.aspetjournals.org at ASPET Journals on April 19, 2024

Fig. 2

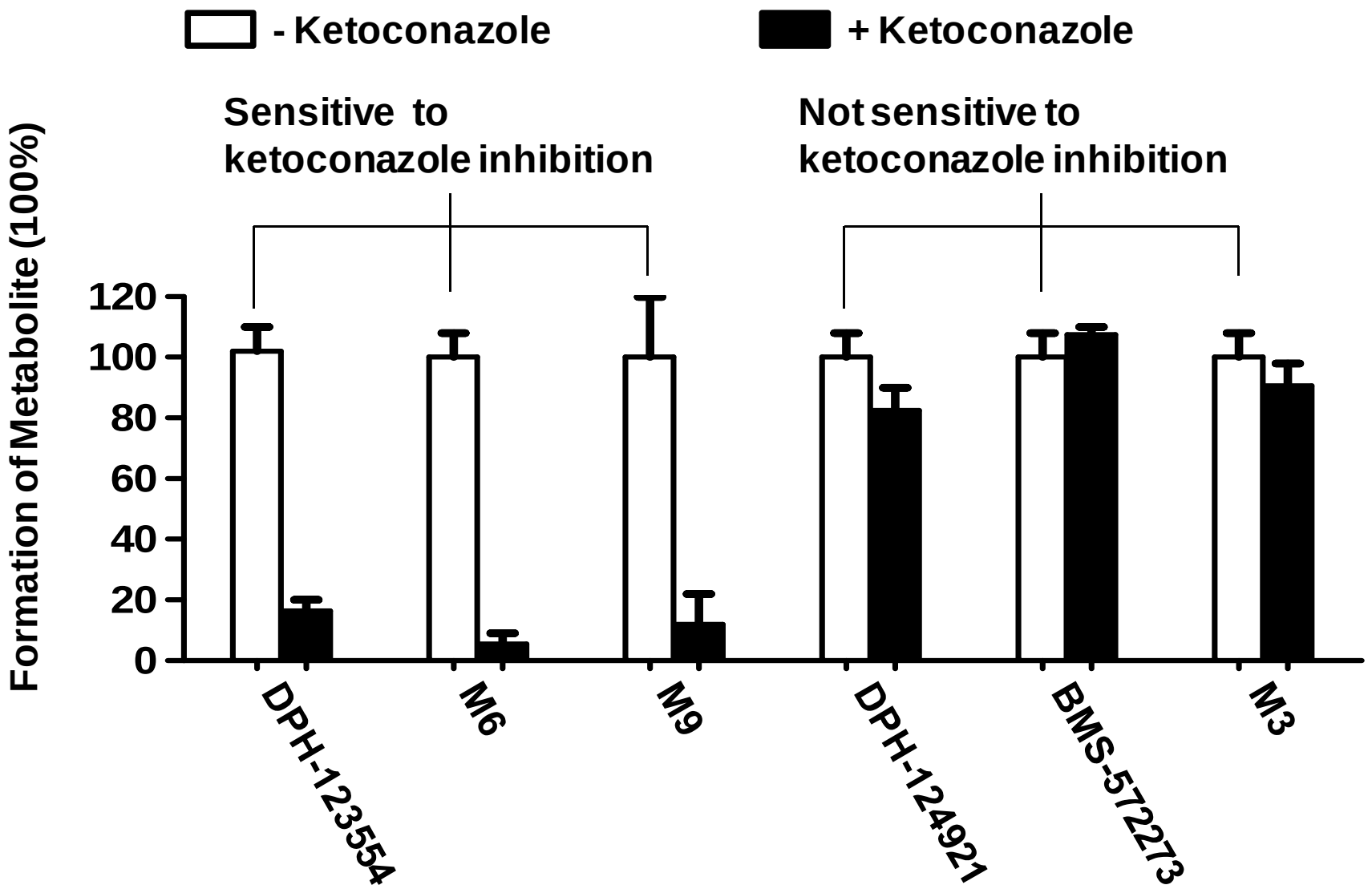

DMD Fast Forward. Published on March 1, 2012 as DOI: 10.1124/dmd.111.043596
This article has not been copyedited and formatted. The final version may differ from this version.

Downloaded from dmd.aspetjournals.org at ASPET Journals on April 19, 2024

Fig. 3

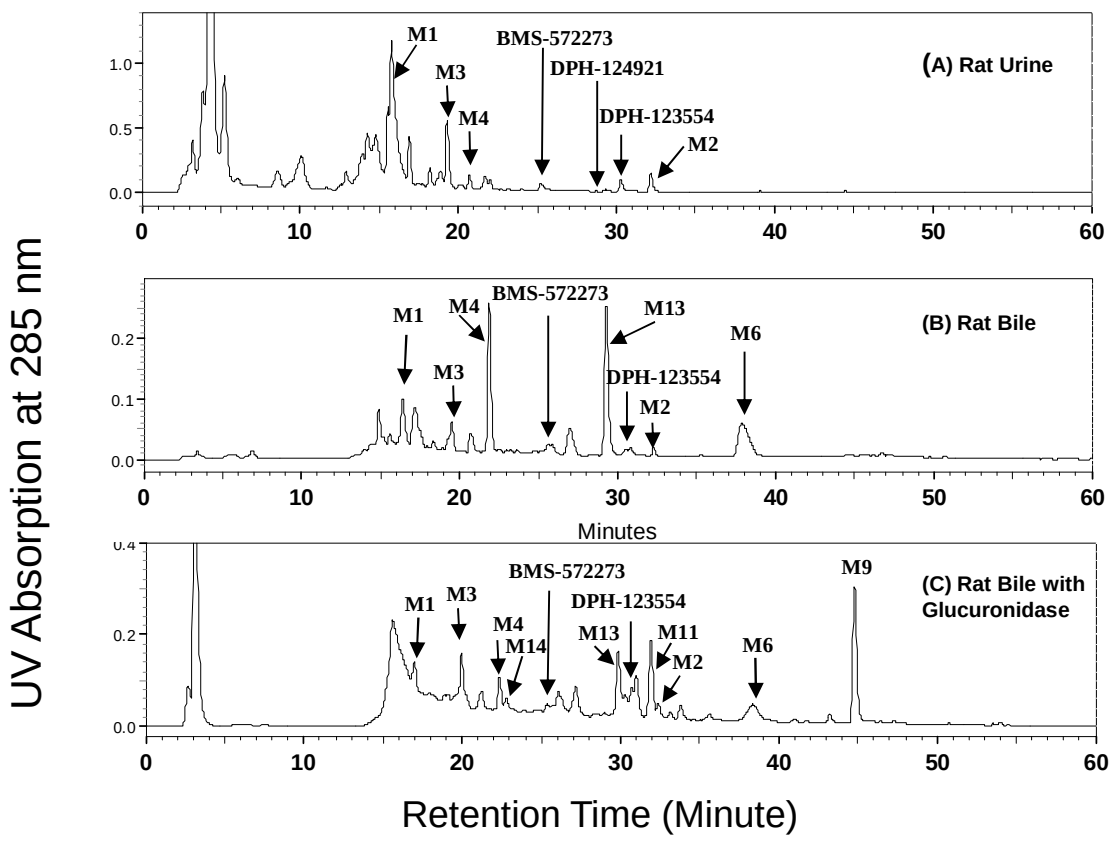

DMD Fast Forward. Published on March 1, 2012 as DOI: 10.1124/dmd.111.043596
This article has not been copyedited and formatted. The final version may differ from this version.

Downloaded from dmd.aspetjournals.org at ASPET Journals on April 19, 2024

Fig. 4

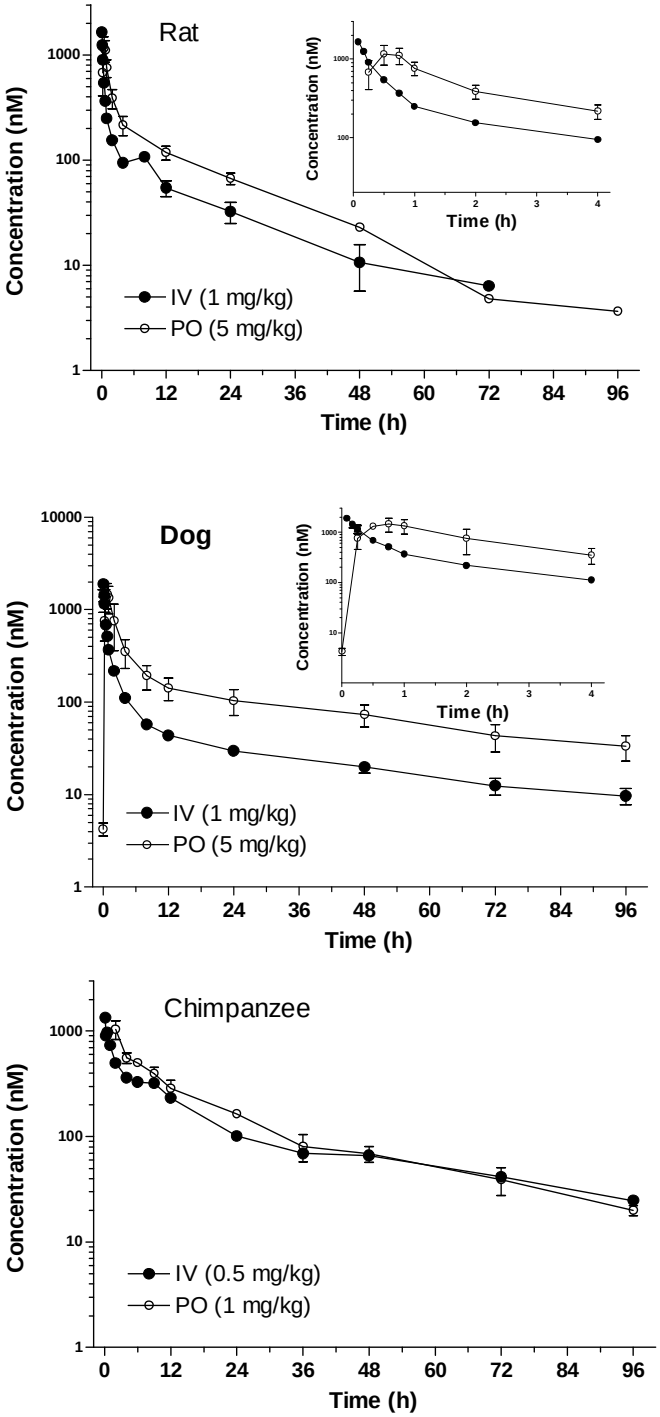

DMD Fast Forward. Published on March 1, 2012 as DOI: 10.1124/dmd.111.043596
This article has not been copyedited and formatted. The final version may differ from this version.

Downloaded from dmd.aspetjournals.org at ASPET Journals on April 19, 2024

Fig. 5

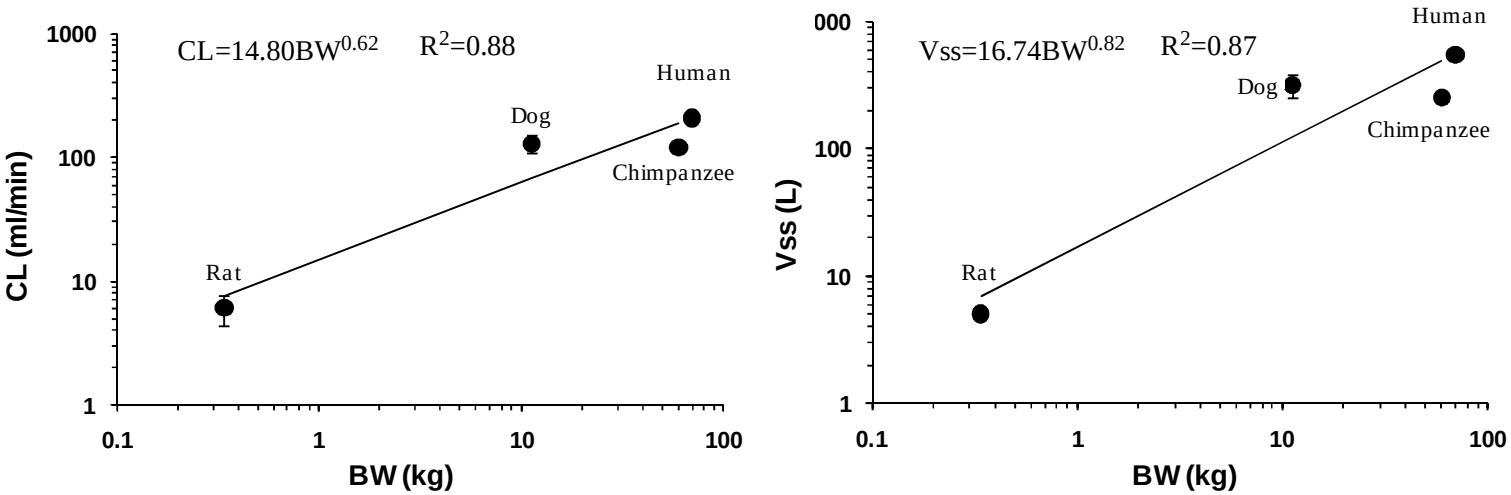

DMD Fast Forward. Published on March 1, 2012 as DOI: 10.1124/dmd.111.043596
This article has not been copyedited and formatted. The final version may differ from this version.

Downloaded from dmd.aspetjournals.org at ASPET Journals on April 19, 2024

Fig.6

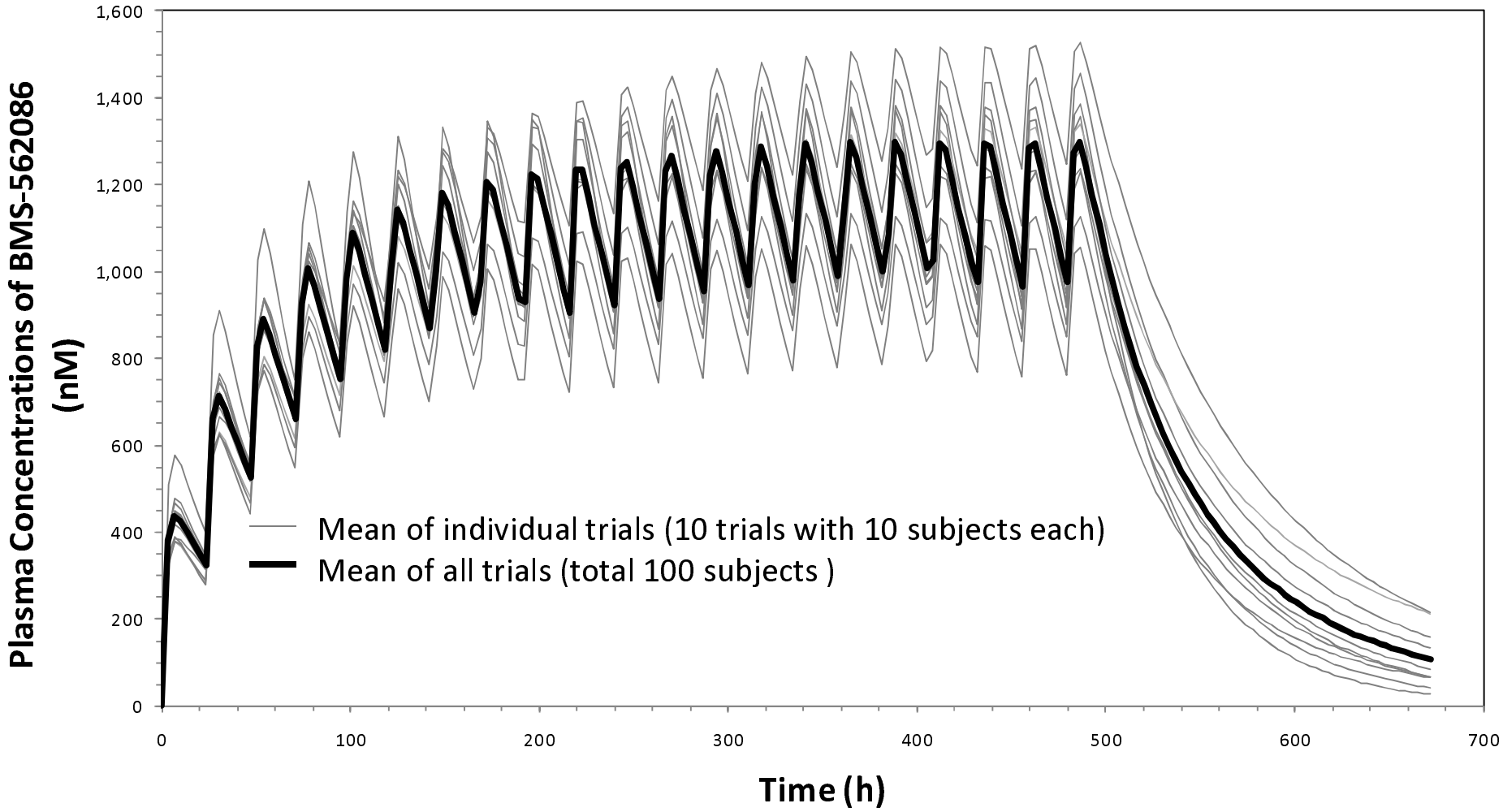

DMD Fast Forward. Published on March 1, 2012 as DOI: 10.1124/dmd.111.043596
This article has not been copyedited and formatted. The final version may differ from this version.

Downloaded from dmd.aspetjournals.org at ASPET Journals on April 19, 2024

Fig. 7

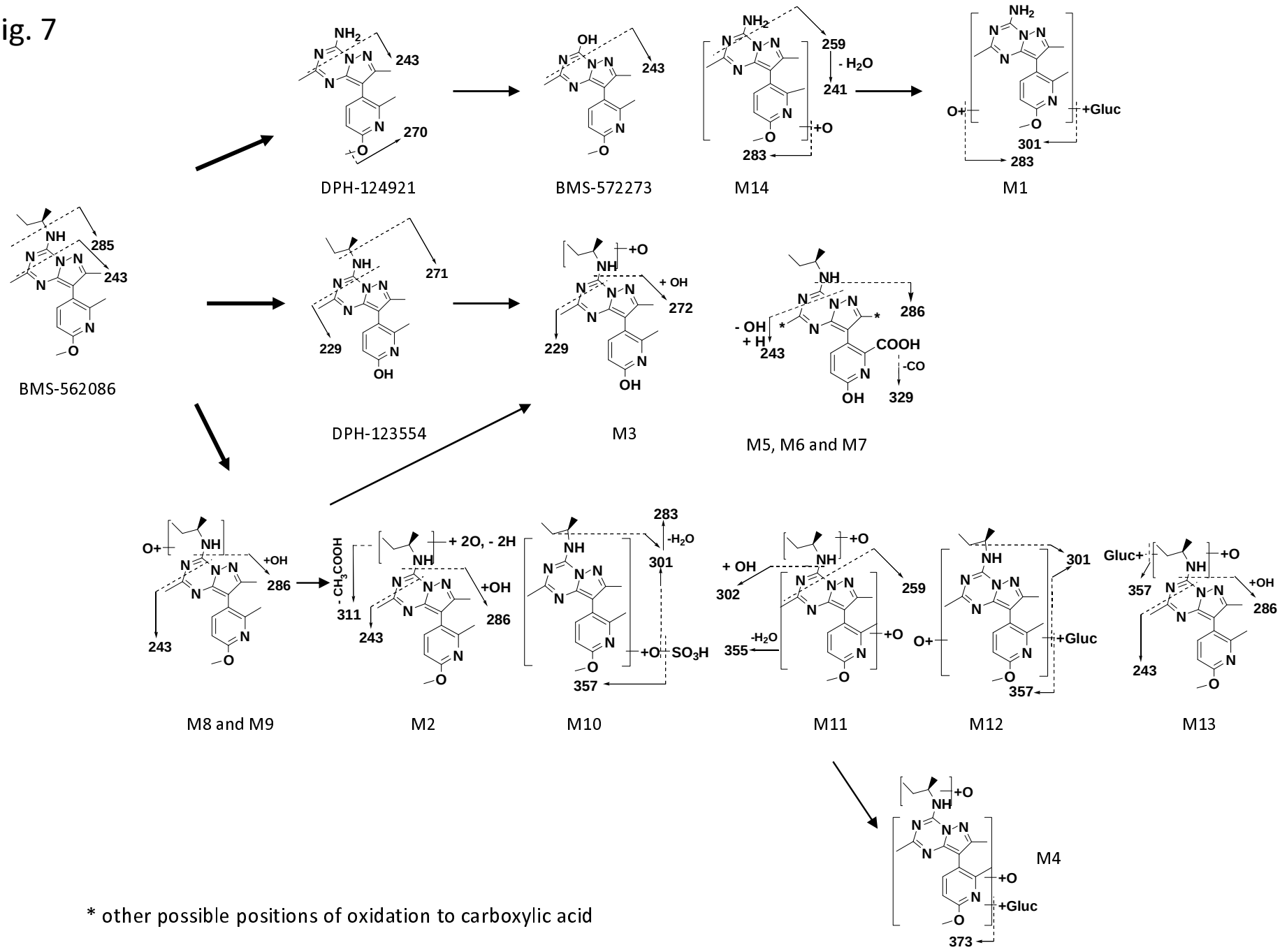

DMD Fast Forward. Published on March 1, 2012 as DOI: 10.1124/dmd.111.043596
This article has not been copyedited and formatted. The final version may differ from this version.

Downloaded from dmd.aspetjournals.org at ASPET Journals on April 19, 2024